Mechanisms of lipids extraction from skin lipid bilayers by sebum triglycerides†

Anna Sofia Tascini,*[a] Massimo G. Noro,[b‡] John M. Seddon,[a] Rongjun Chen[c] and Fernando Bresme[a]

The skin surface, our first barrier against the external environment, is covered by the sebum oil, a lipid film composed of sebaceous and epidermal lipids, which is important in the regulation of the hydration level of our skin. Here, we investigate the pathways leading to the transfer of epidermal lipids from the skin lipid bilayer to the sebum. We show that the sebum triglycerides, a major component of sebum, interact strongly with the epidermal lipids and extract them from the bilayer. Using microsecond time scale molecular dynamics simulations we identify and quantify the free energy associated with the skin lipids extraction process.

1 Introduction

The skin surface is the outermost protective barrier between our bodies and the external environment. There are three possible routes for external pathogens, particles and molecules to penetrate the skin barrier: transcellular delivery, intercellular delivery (*i.e.* through the skin lipid matrix), and via the skin appendages, namely the hair follicles (appendageal route). The main barrier for absorption in the first two routes is the top layer of the skin, the Stratum Corneum (SC), a dense layer populated by dead cells called corneocytes. The crystalline-like SC lipid matrix[1,2] has a very low permeability, and represents the main barrier against absorption via intercellular pathways. The follicle route, instead, provides a pathway for the permeation of slowly diffusing compounds and high molecular weight assemblies, such as nanoparticles[3,4]. The sebum fills the gap between the hair follicle and the skin, and it is considered to be the main transport route of the follicular pathway[5]. The high permeation ability of follicles has promoted the development of transdermal drug delivery approaches which target this pathway[3,6–8].

The skin surface is coated with a lipid film composed of a mixture of sebaceous lipids (the sebum oil) and a small fraction of epidermal lipids, which can detach from the outermost layer of the skin, the stratum corneum[9,10]. Different parts of the body have different concentrations of sebaceous lipids, for example the forehead and the forearm are examples of sebum-rich areas and sebum-poor areas[11], respectively. The distribution of these areas in our body, is correlated with the location of the hair follicles, since the sebum oil is released onto the surface via these follicles. The sebum oil has been found to play a key role in regulating the hydration and, more generally, waterproofing properties of the skin[12–14]. Sebum oil also features antimicrobial properties[15], and it assists in the transport of antioxidants, such as vitamin E, through the skin[16,17]. Both, the lack (*hyposeborrhea*) and excess (*hyperseborrhea*) of sebum can make the skin more fragile and vulnerable to irritations. Typically, sebum poor areas are often subjected to discomfort and itching, and become more sensitive to all external aggressive agents. Sebum rich areas, instead, have a higher concentration of antioxidants[17].

A microscopic understanding of the skin surface is essential to explain and predict its performance as a barrier for water loss and penetration of foreign molecules via both intercellular[18,19] and appendageal routes[20]. This information will be useful for designing better strategies for transdermal drug delivery.

Molecular dynamics (MD) simulation provides a powerful approach to quantify the interactions between biological molecules, and to disentangle the interaction mechanisms with atomistic resolution[21]. MD has been used to investigate the structure and phase behaviour of a single component SC lipid model in water[22–26]. In addition, more complex mixtures consisting of ceramides, cholesterol and free fatty acids have been investigated to assess the impact of the lipid composition on the permeability, structure and fluidity of the SC membrane[18,27–31]. The permeation of small molecules[19], ethanol[19,32], DMSO[19,22] , oils[33,34] and nanoparticles[35,36] has also been quantified using MD simulations[2]. Most simulations on skin lipids have focused so far on bilayers or stacks of bilayers in contact with water. The role of sebum on permeation and specifically its interactions with skin lipids has not been considered using MD simulations. Such study is needed, since there is experimental evidence showing that the

[a] *Department of Chemistry, Imperial College London, UK; E-mail: ast14@ic.ac.uk, fbresme@imperial.ac.uk*

[b] *Unilever R&D Port Sunlight, Quarry Road East, Bebington, Wirral, CH63 3JW, UK.*

‡ *Present address: Science and Technology Facility Council (STFC), Daresbury Laboratory, Sci-Tech Daresbury, Keckwick Lane, Daresbury, Warrington, WA4 4AD*

[c] *Department of Chemical Engineering, Imperial College London, UK.*

† Electronic Supplementary Information (ESI) available: [details of any supplementary information available should be included here]. See DOI: 10.1039/cXCP00000x/

interactions between the SC and the sebum oil can be significant to determine the properties of the lipid film of the skin surface [10].

We recently proposed a computer simulation model of the sebum oil, consisting of triglycerides, and used this model to investigate the triglyceride-water interactions [14]. Building on this model, using atomistic MD simulations, here we study the interaction between sebum triglycerides (TG) and a multicomponent model of the skin. The latter incorporates the three most abundant constituents of the stratum corneum: ceramide 2 (CR2), cholesterol (CHO) and free fatty acids (FFA), here represented by lignoceric acid. In our study we uncover the penetration mechanisms of TG into the membrane and identify different pathways for lipid extraction from the SC membrane to the sebum. We propose that these pathways define the routes followed by SC lipids when they are extracted from the bilayer, and they might explain the presence of SC lipids in the sebum films coating the skin surface, previously reported in *in vivo* experiments on human skin [10].

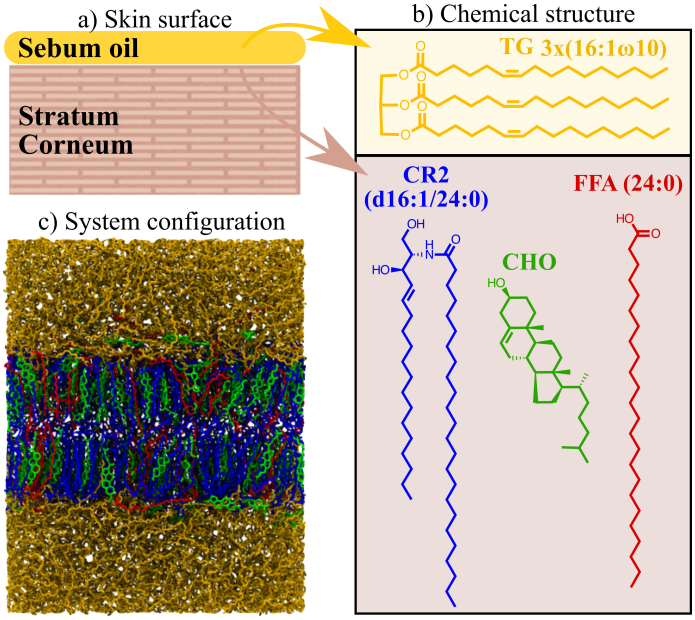

Fig. 1 a) Schematic representation of the top of the skin surface, showing how the sebum oil interacts with lipids at the outermost layer of the skin, the stratum corneum **b)** Chemical structure of the lipids investigated in this work. The sebum is modelled with its most abundant component, the triglyceride tri-cis-6-hexadecenoin (TG). The multicomponent model of the SC is made up of ceramide 2 (CR2), cholesterol (CHO) and lignoceric acid (FFA). **c)** Representative snapshot of the system used in this work. The colour code is the same as that of the chemical structures on the right panels.

2 Methods

2.1 Input configurations and simulation details

Molecular Dynamics simulations have been used to investigate the interactions between the main component of the human sebum oil (triglyceride tri-cis-6-hexadecenoin - TG), and SC lipids. All the simulations were performed using the GROMACS/4.5.5 molecular simulation package [37].

Following previous studies [2,23,38,39], the stratum corneum lipid matrix was modelled with a ternary mixture of the main three components: ceramide 2 (CR2), cholesterol (CHO) and lignoceric acid (FFA). Their chemical structures are shown in Fig. 1-b. A molar ratio of CR2:CHO:FFA equal to 2:2:1 was used to ensure the structural and mechanical properties of healthy skin [27].

The SC membrane was constructed using the open source software Packmol [40] to place 288 SC lipid molecules in each of the two leaflets of a bilayer, symmetrically about the bilayer midplane as specified in ESI (see Fig. S1). The system was then equilibrated in water, with the same procedure as described in ref. 27.

Following the approach of our previous work (see ref. 14), the human sebum was represented by the triglyceride tri-cis-6-hexadecenoin. The chemical structure of a TG molecule is shown in Fig. 1-b. Starting from an equilibrated configuration of SC bilayer in water, the solvent molecules were replaced with two sebum slabs, made up of 256 TG molecules each. The TG slabs were then equilibrated for 300 ns following the procedure described in ref. 14. The final SC-TG configuration is shown in Fig. 1-c.

We used the Berger *et al.* [41] forcefield to describe the bonded and non-bonded interactions of the lipid molecules. This forcefield has been used in many simulations of skin lipids [23,32,38,42]. It is based on the OPLS [43] and GROMOS87 [44] forcefields and includes the Ryckaert-Bellemans dihedral potential [45] to model the hydrocarbon chains. The unsaturated region of the acyl tails of the TG molecule was modelled using the Berger's description of the double bond for the POPC molecule [46] and the *cis* geometry was enforced using a dihedral potential. van der Waals interactions were truncated at 1.2 nm and electrostatic interactions were computed in full using the Particle Mesh Ewald algorithm [47]. The intra-molecular bonds were constrained using the P-LINCS [48] algorithm and periodic boundary conditions were applied in all directions.

The first step to equilibrate the SC-TG configuration was a 500 ps equilibration in the *NVT* ensemble setting the velocity rescaling algorithm [49] to a temperature of $T = 310\,\mathrm{K}$ (to mimic the physiological temperature of the skin), using a time coupling constant, τ, of 0.1 ps. This was followed by a 400 ns run in the *NPT* ensemble, with the Nosé-Hoover thermostat, with $T = 310\,\mathrm{K}$ and $\tau = 1\,\mathrm{ps}$, and the Parinello-Rahaman barostat, applied semi-isotropically with $p = 1\,\mathrm{bar}$, $\tau = 5\,\mathrm{ps}$ and compressibility $4.5 \times 10^{-5}\,\mathrm{bar}^{-1}$. The production run was extended for $2\,\mu\mathrm{s}$ in the *NPT* ensemble at the same conditions. The time-step of the simulations was set equal to 0.002 ps. We found that all the parameters converge after an equilibration time of $\approx 0.75\,\mu\mathrm{s}$. In particular, we monitored the time dependence of the number of CR2, CHO, and FFA in the bilayer (see section S5.1 in ESI), area per lipid (see section S5.2 in ESI), hydrogen bonding (see section S5.3 in ESI).

2.2 Tracking the extraction mechanisms

The numbers of TG insertions and lipids extractions were obtained through the method explained below, which was implemented in an in-house code.

The centre of the bilayer was calculated, as described in ESI (see Fig. S2), in order to define two slices parallel to the *xy* plane at a specified height, d_{SLICE}, above and below the bilayer mid

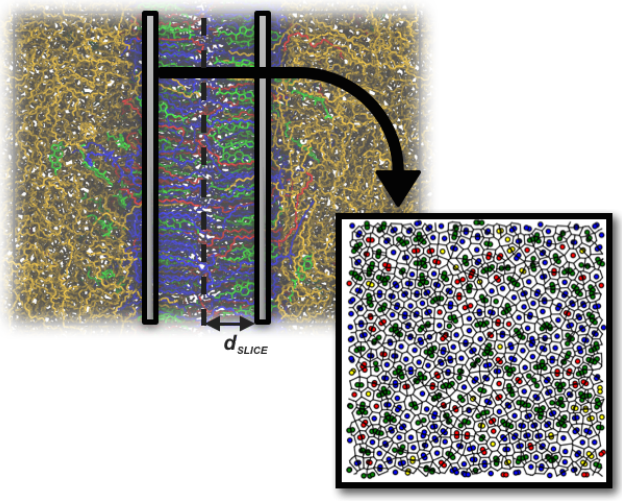

Fig. 2 The position of the slices used to determine the number of extraction events is shown on a representative system configuration. The inset shows the section of the bilayer used to determine the position and configuration of the molecules.

plane. A graphical example of the definition of the slices is shown in Fig. 2. The height, d_{SLICE}, was set to 1.45 nm, so that the slices were just below the head group planes. The slice thickness must be larger than the largest bond length for molecules within the bilayer to ensure that if the slice passes though a molecule, at least one of the molecules' atoms are within the slice volume. In this analysis it was set to 0.15 nm.

The atoms inside each slice are recorded as shown in Fig. 2, and individual molecules are assigned to one of the two leaflets or to the TG phase by checking whether at least one of their atoms was inside or outside the slices. Specifically, if a SC lipid molecule does not have atoms in either of the two slices, it is assigned as being outside the bilayer and one extraction event is counted. If a TG molecule is found to be in one of the slices it is considered to be anchored to the bilayer. For molecules with more than one chain, *i.e.* TG and CR2, each chain is considered separately in order to assign part of the molecule to the bilayer or the TG phase, based on the positions of the atoms in the chain. The resulting configuration of TG or CR2 molecules is then determined by considering the relative assignment of the individual chains, as specified in ESI.

2.3 Free energy pathway of lipid extraction

The free energy for lipid extraction from the bilayer to the sebum phase can be estimated by analysing the density distribution of the SC lipids.

From the coordinates of the head group atoms along the simulation box, it is possible to determine and estimate the probability of the atoms visiting a particular z coordinate, $Z(i) = \frac{\overline{\rho}(z)}{\overline{\rho}(0)}$, where $\overline{\rho}(z)$ is the average number of lipids at a particular height, z, and $\overline{\rho}(0)$ indicates the number of lipids in the reference state, which we locate at the minimum of the distribution. The free energy profile, ΔG, can therefore be obtained from $Z(i)$, as

$$\Delta G(z) = G(z) - G(0) = -k_B T \ln\left(\frac{\overline{\rho}(z)}{\overline{\rho}(0)}\right). \quad (1)$$

Another important parameter for the characterisation of the extraction process is the tilt angle, θ_T, of the lipids. The tilt angle has been found to be critical in explaining intra-leaflet dynamics in lipid membranes, *e.g.* cholesterol flip-flop[50]. The tilt angle of CHO and FFA molecules, along with the position of the head group, were used as reaction coordinates to build the 2D energy landscape, $\Delta G(\rho(z), \theta_T)$, of lipid extraction and to discuss the mechanism of extraction from the bilayer, as reported below.

One head group atom for each species was selected to track the position of the lipids along z, specifically O21 for CR2, O6 for CHO, O1 for FFA (see Fig. 3 for labels). The tilt angle is defined as the angle between the lipid molecular axis and the z axis. The molecular axis of CHO was defined as the vector between atoms C5 and C21, *i.e.* the axis of the rigid ring structure. The FFA molecular axis was defined, instead, from the carbon atoms at the ends of the acyl chain, C1 and C24 (see Fig. 3 for labels).

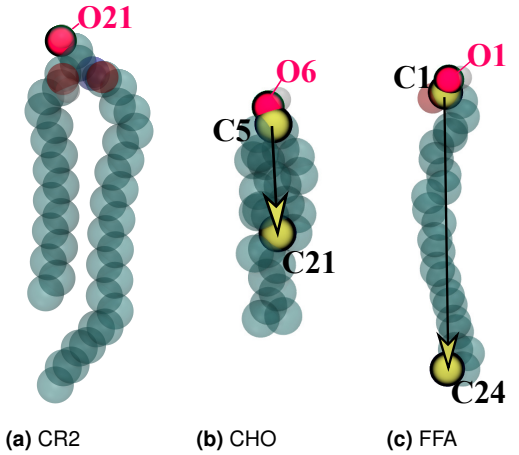

Fig. 3 (a) CR2 molecule with atom labels for O21 (b) CHO molecule with atom labels for O6, C5 and C21. (c) FFA molecule with atom labels for O1, C1 and C24.

3 Results and Discussion

Representative simulation snapshots illustrating the different interdigitation modes between TG and SC lipids that we identified, are shown in Fig. 4. The different mechanisms are represented in coloured boxes. Each of the four molecular species present in these simulations show very different behaviour in the sebum-SC system and each is described and further characterised in the following.

3.1 TG anchoring

A number of TG molecules (≈ 20 insertions in each leaflet) anchor to the SC bilayer via their acyl chains, corresponding to a fractional concentration of TG in the bilayer of ≈ 0.1 TG chains per SC lipid. The evolution of the number of insertion events *vs.* time in the top and bottom leaflets and the criterion used to define the anchoring can be found in Fig. S6-a and section S2 in the ESI. The most common type of anchoring ($\approx 89.7\%$ of the TG molecules)

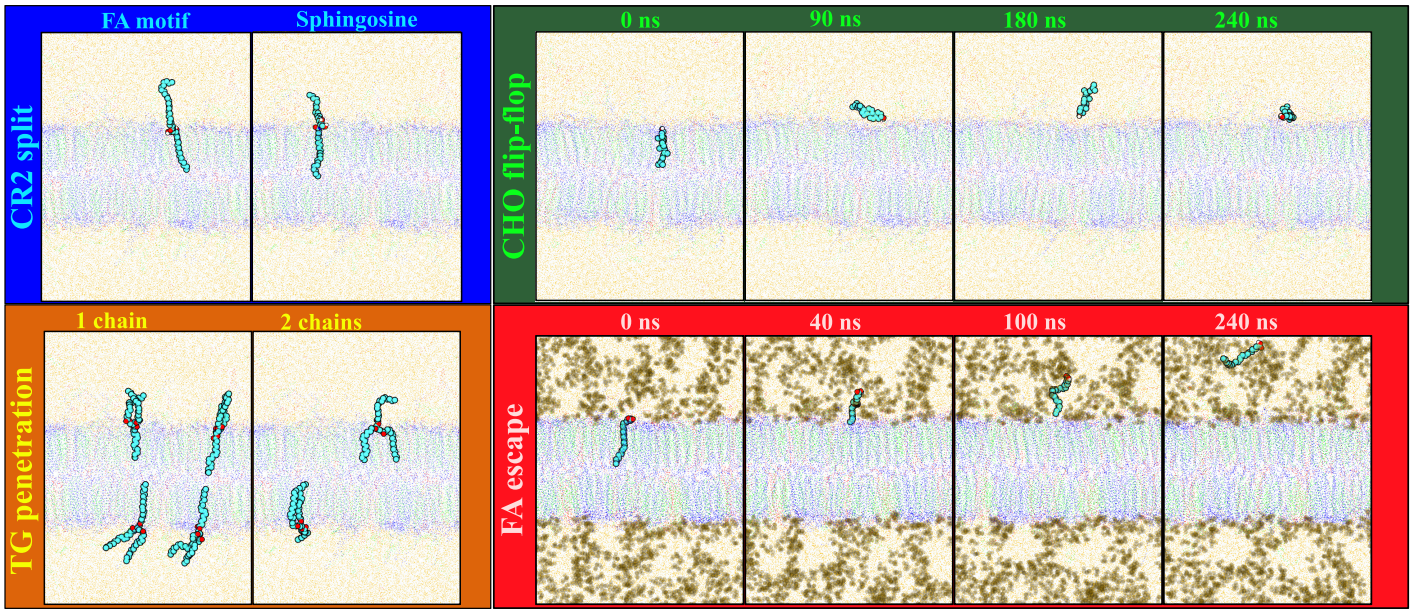

Fig. 4 Representative snapshots illustrating the main mechanisms of SC lipids-sebum interaction. The behaviour of each lipid species is represented in a separate coloured box. Blue box: CR2 splitting, with either the fatty acid (left) or the sphingosine (right) motif in the oily layer; orange box: TG penetration with one (left) or two (right) chains inserted into the SC bilayer; green box: CHO flip-flop at different times (from left to right: 0, 90, 180, 240 ns); red box: the extraction of FFA at different times (from left to right: 0, 40, 100, 240 ns). Representative simulation trajectories illustrating these mechanisms are available in the ESI.

involves the insertion of one of the three chains, as shown in the left-hand side orange box of Fig. 4. Anchoring via the penetration of two chains (see right-panel in orange box in Fig. 4) is also observed, although much less frequently ($\approx 10\%$). These results are consistent with the assumption that the multi-tail penetration might involve a higher energy barrier, connected to the required alignment of two chains and the concomitant increase of the area of the bilayer.

Several methods to classify the conformations of triglyceride molecules are available in literature[14,51,52]. Here, the preferential conformations of the TG molecules were analysed with the method reported in ref. 14 and ESI (see section S2). This criterion identifies the dominant conformations that are consistent with previous studies[51,52] and enables a direct comparison with the analysis of sebum TG interacting with water[14]. Fig. 5 shows the 3D distributions of TG conformations as a function of the three angles described by the mutual orientation of the chains: θ_{12}, θ_{23} and θ_{13} for anchored TG molecules (bottom graph) and non-anchored TG molecules (top-graph). The analysis confirms that, the "tuning fork" shape, with two chains in the sebum phase and the central chain inserted into the bilayer, is the dominant configuration. This configuration was also found to be the dominant one in bulk TG[14].

3.2 CR2 splitting

The CR2 molecules in contact with the sebum layer, are generally very stable in the bilayer. After $2\,\mu s$ we found that only $\approx 1\%$ of lipids left the bilayer, and adsorbed at the TG-SC interface (see Fig. S9 in ESI). The retention in the bilayer and the adsorption is facilitated by the strong hydrogen-bond network formed by the

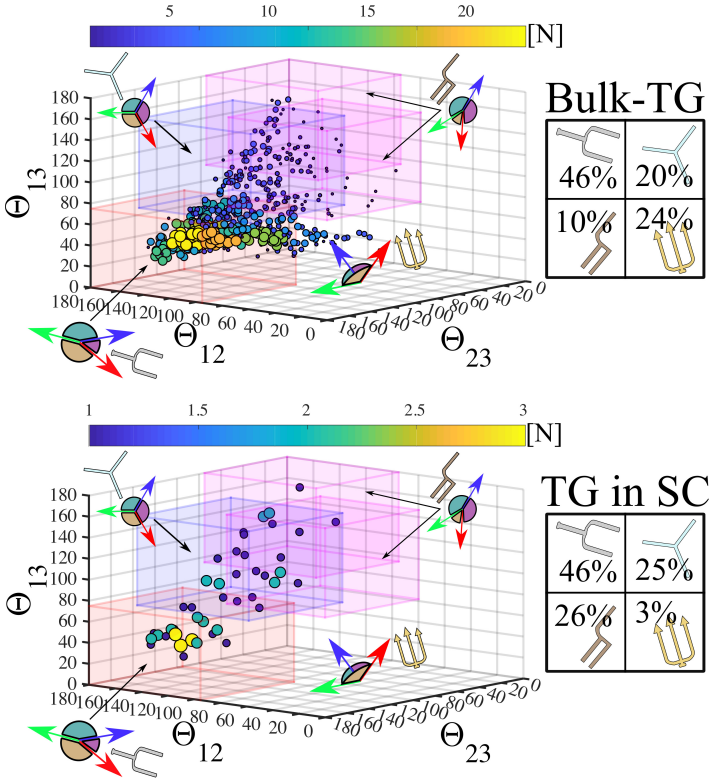

Fig. 5 3D distribution of triglyceride conformations as a function of the three angles described by the mutual orientation of the chains: θ_{12}, θ_{23} and θ_{13}, for bulk TG (top) and TG in SC bilayer (bottom). The definition of the region associated with each shape is available in ESI and in ref. 14. The tables next to the 3D-histograms summarise the % of occurrence of the different shapes.

CR2 head groups. This network has been previously observed and discussed in several simulation studies[22,33,38,39] and in the ESI (see section S5.3). A higher fraction of CR2 lipids ($\approx 11\%$) partially detach from the bilayer, with one of the aliphatic chains remaining within the bilayer while the other moves to the sebum, resulting in an angle of $\approx 180^\circ$ between the two chains (see blue box in Fig. 4). We define this event as "CR2 splitting". We have quantified the number of CR2 splitting events *vs.* time by differentiating between conformations where the chain detaching from the bilayer is the free fatty acid or the spinghosine (see Fig. S6-a in the ESI). Our analysis shows that the free fatty acid motif is three times more likely to be involved in the splitting event. This observation can be rationalized by considering the asymmetry of the CR2 tails. When the longer fatty acid chain bends in the head-group region[22], the energy penalty for the splitting event to occur is lower and the free fatty acid chain penetrates into the oily layer (see Fig. S6-b in the ESI).

3.3 CHO flip-flop and FFA escape

The sebum extracts a significant number of CHO and FFA lipids ($\approx 15\%$ of the lipid molecules originally placed in the bilayer, as shown in Fig. S9 in the ESI). The mole fractions of SC lipids (distinguishing the contribution of CHO and FFA) in the sebum phase, X_{SC}, with respect to the total number of lipids in the oily phase, $X_{SC} = N_{SC}/(N_{TG}+N_{SC})$, are reported in Table 1.

Table 1 Mole fractions of SC lipids (CHO and FFA) extracted and dispersed in the TG phase.

SC	X_{SC}
CHO	0.06
FFA	0.04

The extraction mechanisms of these two lipids are very different. The CHO molecules preferentially leave the bilayer through a flip-flop like event (see green box in Fig. 4), with the CHO molecules reversing their orientation before adsorbing at the SC bilayer interface. Specifically, CHO first lies flat at the SC-sebum interface and from there can either insert into the sebum or back into the bilayer. In Fig.6-left, we show a representative snapshot from the simulations where the extracted CHO molecules (in green) are mostly found at the TG-SC interface.

Most FFA lipids are extracted directly without undergoing a flip-flop-like event, diffusing straight into the TG phase (see red box in Fig. 4). The extraction pathway of FFA is similar to that of the fatty acid tails of the CR2 lipids. Due to the long acyl chain (counting 24 carbon atoms), the FFA aliphatic tail bends near the carboxylic acid group at the bilayer-TG interface (see the first snapshot in the red box in Fig. 4). The bending allows a closer interaction between the OH group in FFA and the glycerol groups (GLY) of TG . We have shown previously that the GLY in TG molecules interact strongly with each other and form percolating networks[14]. At the SC bilayer surface the formation of this network is partially inhibited due to the direct interaction between SC and TG lipids. In Fig. 6-left we show the clusters of TG GLY groups using different colours (see ESI for information about the clustering criteria and colour legend). The picture shows how the sites where the TG network meet the bilayer serve as pathway for FFA escape. Once extracted to the sebum phase, FFA OH groups interact with the GLY-clusters and the acyl chains, dragged behind, are placed in the space occupied by the TG aliphatic tails.

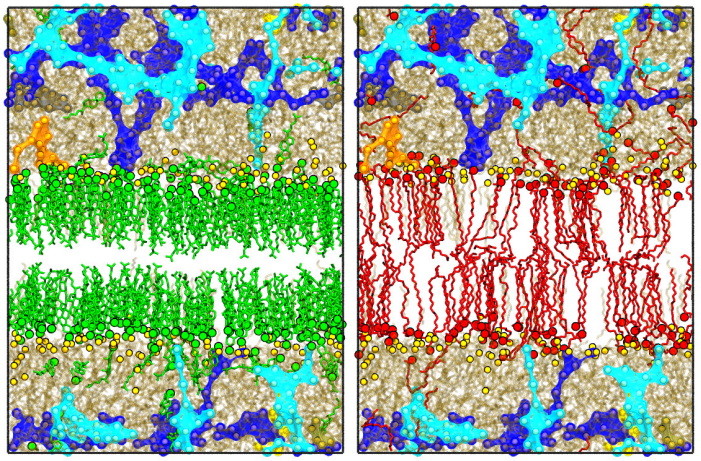

Fig. 6 Representative snapshots from the simulation. All the lipid head groups are represented as a spherical bead and the tails as sticks of different colours: green for CHO (left panel), red for FFA (right panel) and yellow for TG (left and right panel). The formation of GLY clusters is highlighted with coloured surfaces that bridge all the glycerol groups belonging to the same cluster. We distinguish different clusters by using different colours, *i.e.* blue, light-blue, orange, yellow and grey. Left) TG and CHO molecules in the bilayer and in the oil phase. Most of the extracted CHO are absorbed at the TG-SC interface. Other SC lipids (CR2 and FFA) are omitted for clarity. Right) Snapshot showing representative location of the TG and FFA lipids within the system. Most of the FFA head groups extracted from the bilayer interact directly with the GLY network. Other SC lipids (CR2 and CHO) are omitted for clarity.

As explained in the Methods sections, the extraction events can be monitored throughout our microsecond simulations and the free energy differences can be quantified using $\Delta G(z,\theta_T) = -k_BT \ln\left(\rho(z,\theta_T)/\rho_{0,0}\right)$ where $\rho(z,\theta_T)$ is the number of lipid head groups with z coordinate normal to the bilayer surface and tilt angle θ_T, with respect to the axis normal to the bilayer plane. This multivariate free energy landscape can be used to quantify the energy cost associated with the extraction of the lipids from the bilayer. $\rho_{0,0}$ is taken as a reference for the free energy. We choose (z,θ_T) of the lipids placed in the bilayer as a reference (see labels T and B in Fig.7). The free energy densities are reported in k_BT units and shown in Fig.7. The free energy surface features two well defined energy basins, T and B, which correspond to stable conformations of the CHO and FFA lipids in the bilayer. The CHO molecules are preferentially tilted with average angles, $\theta_T \approx 8^\circ$ and 172° relative to the bilayer normal, while the FFA lipid tilt angles are $\theta_T \approx 15^\circ$ and $\theta_T \approx 165^\circ$. These tilt angles agree with previous simulation studies of SC lipid bilayers[39].

The energy cost associated with the extraction process from the stable basins T and B is 4 k_BT and 3.5 k_BT for CHO and FFA, respectively. These values define the partitioning of the lipids between the sebum phase and the bilayer. Our model predicts, $\rho_{CHO,sebum}/\rho_{CHO,SC} = \exp(-\Delta F/k_BT) = 0.02$ and $\rho_{FFA,sebum}/\rho_{FFA,SC} = \exp(-\Delta F/k_BT) = 0.03$.

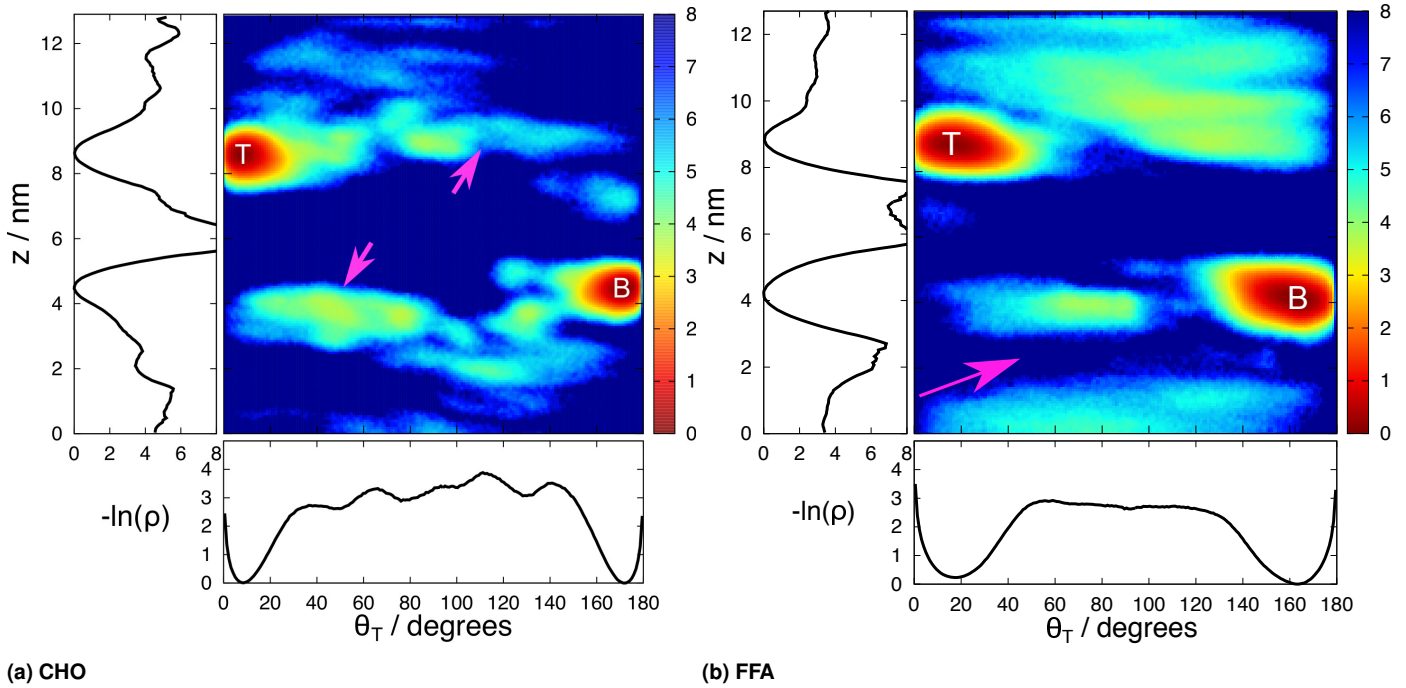

Fig. 7 2D Free energy landscape for (a) CHO and (b) FFA extraction as a function of tilt angle and head group z coordinate. The 1D plots are also reported on the *x* and *y* axes. The colour bar represents the free energy in k_BT. Letters T and B correspond to the top and bottom leaflets in the bilayer. (a) The magenta arrows indicate CHO flip-flopping to the TG phase, but maintaining contact with the bilayer. (b) Here the magenta arrow shows the activation energy barrier.

The partitioning of FFA in the sebum phase is more homogeneous than that of CHO (*c.f.* free energy densities at $z > 8$ nm and $z < 4$ nm in the left and right panels shown in Fig. 7), reflecting the fact that CHO adsorbs preferentially at the SC bilayer with a tilt angle of 90° (see magenta arrows in the left panel of Fig. 7), while the FFA lipids detach and disperse in the sebum phase. Interestingly, we find that the FFA extraction can occur via an activation barrier or not. In the region below the lower leaflet ($z < 4$ nm) we observed an activation barrier of $\sim 7k_BT$ units (see magenta arrow in Fig. 7). This difference is related to the TG glycerol group network arrangement, which is not perfectly symmetric around the bilayer (as also shown in Fig. 6, and Fig. S8 in ESI).

4 Conclusions

In summary, we have investigated the interactions between sebum TGs and SC lipid bilayers using atomistic simulations. Our computations confirm that the sebum extracts epidermal lipids by TG anchoring at the interface. The preferential conformation of TG molecules is the tuning fork (≈ 50% of the molecules in the system), as in bulk TG[14]. CR2 molecules remains stable inside the bilayer, while CHO lipids remain mostly adsorbed at the SC bilayer upon extraction and the FFA lipids detach from the bilayer dissolving into the sebum phase by interacting with the TG glycerol group network. Our model predicts that the free energies associated with the extraction are of the order of $\sim 4k_BT$, indicating a small concentration of SC lipids in the skin surface lipid film. Our investigation of symmetric SC bilayers suggests that the outermost layers of SC lipids, closer to the skin surface, might preserve their integrity despite the presence of the sebum oil. Further experimental and computational studies are required to shed more light into the role that the SC lipid–sebum interactions have on the properties of the skin.

5 Acknowledgements

This work has been funded by the EU 7th Framework Programme, ITN-SNAL. We also acknowledge the EPSRC grants, EP/J017566 and EP/J003859/1. We thank Imperial College High Performance Computer Service for the computational resources.

Conflicts of interest

There are no conflicts to declare.

References

1 L. Norlén, *International journal of cosmetic science*, 2006, **28**, 397–425.
2 R. Notman and J. Anwar, *Advanced Drug Delivery Reviews*, 2013, **65**, 237–250.
3 J. Lademann, H. Richter, S. Schanzer, F. Knorr, M. Meinke, W. Sterry and A. Patzelt, *European Journal of Pharmaceutics and Biopharmaceutics*, 2011, **77**, 465–468.
4 M. Schneider, F. Stracke, S. Hansen and U. F. Schaefer, *Dermato-Endocrinology*, 2009, **1**, 197–206.
5 P. Kattou, G. Lian, S. Glavin, I. Sorrell and T. Chen, *Pharmaceutical Research*, 2017, **34**, 2036–2048.
6 A. Patzelt and J. Lademann, *Expert Opinion on Drug Delivery*, 2013, **10**, 787–797.
7 M. Morgen, G. W. Lu, D. Du, R. Stehle, F. Lembke, J. Cer-

vantes, S. Ciotti, R. Haskell, D. Smithey, K. Haley and C. Fan, *International Journal of Pharmaceutics*, 2011, **416**, 314–322.

8 S. Jung, N. Otberg, G. Thiede, H. Richter, W. Sterry, S. Panzner and J. Lademann, *Journal of Investigative Dermatology*, 2006, **126**, 1728–1732.

9 R. S. Greene, D. T. Downing, P. E. Pochi and J. S. Strauss, *Journal of Investigative Dermatology*, 1970, **54**, 240–247.

10 H. M. Sheu, S. C. Chao, T. W. Wong, J. Y. Y. Lee and J. C. Tsai, *British Journal of Dermatology*, 1999, **140**, 385–391.

11 D. T. Downing and J. S. Strauss, *Journal of Investigative Dermatology*, 1974, **62**, 228–244.

12 K. R. Smith and D. M. Thiboutot, *The Journal of Lipid Research*, 2007, **49**, 271–281.

13 C. C. Zouboulis, M. Picardo, Q. Ju, I. Kurokawa, D. Törőcsik, T. Bíró and M. R. Schneider, *Reviews in Endocrine and Metabolic Disorders*, 2016, **17**, 319–334.

14 A. S. Tascini, M. G. Noro, R. Chen, J. M. Seddon and F. Bresme, *Phys. Chem. Chem. Phys.*, 2018, **20**, 1848–1860.

15 M. Lovászi, A. Szegedi, C. C. Zouboulis and D. Törőcsik, *Dermato-Endocrinology*, 2017, **9**, e1375636.

16 J. W. Fluhr, M. Mao-Qiang, B. E. Brown, P. W. Wertz, D. Crumrine, J. P. Sundberg, K. R. Feingold and P. M. Elias, *Journal of Investigative Dermatology*, 2003, **120**, 728–737.

17 J. J. Thiele, S. U. Weber and L. Packer, *Journal of Investigative Dermatology*, 1999, **113**, 1006–1010.

18 M. Lundborg, A. Narangifard, C. L. Wennberg, E. Lindahl, B. Daneholt and L. Norlén, *Journal of Structural Biology*, 2018, **203**, 149–161.

19 M. Lundborg, C. L. Wennberg, A. Narangifard, E. Lindahl and L. Norlén, *Journal of Controlled Release*, 2018, **283**, 269–279.

20 J.-C. Tsai, C.-C. Lu, M.-K. Lin, J.-W. Guo and H.-M. Sheu, *Skin pharmacology and physiology*, 2012, **25**, 124–32.

21 J. W. Carter, A. S. Tascini, J. M. Seddon and F. Bresme, *Computational Tools for Chemical Biology*, The Royal Society of Chemistry, 2018, ch. 2, pp. 39–68.

22 R. Notman, W. K. den Otter, M. G. Noro, W. J. Briels and J. Anwar, *Biophysical Journal*, 2007, **93**, 2056–2068.

23 C. Das, P. D. Olmsted and M. G. Noro, *Soft Matter*, 2009, **5**, 4549–4555.

24 S. Guo, T. C. Moore, C. R. Iacovella, L. A. Strickland and C. McCabe, *Journal of Chemical Theory and Computation*, 2013, **9**, 5116–5126.

25 C. M. Macdermaid, R. H. Devane, M. L. Klein and G. Fiorin, *Journal of Chemical Physics*, 2014, **141**, 1–9.

26 T. C. Moore, R. Hartkamp, C. R. Iacovella, A. L. Bunge and C. McCabe, *Biophysical Journal*, 2018, **114**, 113–125.

27 C. Das, M. G. Noro and P. D. Olmsted, *Biophysical Journal*, 2009, **97**, 1941–1951.

28 C. Das, M. G. Noro and P. D. Olmsted, *Physical Review Letters*, 2013, **111**, 1–5.

29 T. C. Moore, C. R. Iacovella, R. Hartkamp, A. L. Bunge and C. McCabe, *Journal of Physical Chemistry B*, 2016, **120**, 9944–9958.

30 J.-W. Guo, T.-K. Lin, C.-H. Wu, K.-C. Wei, C.-C. E. Lan, A. C.-Y. Peng, J.-C. Tsai and H.-M. Sheu, *Journal of Dermatological Science*, 2015, **78**, 34–43.

31 R. Gupta and B. Rai, *The Journal of Physical Chemistry B*, 2015, **119**, 11643–11655.

32 R. Thind, D. W. O'Neill, A. Del Regno and R. Notman, *Chem. Commun.*, 2015, **51**, 5406–5409.

33 A. Akinshina, C. Das and M. G. Noro, *Phys. Chem. Chem. Phys.*, 2016, **18**, 17446–17460.

34 M. I. Hoopes, M. G. Noro, M. L. Longo and R. Faller, *Journal of Physical Chemistry B*, 2011, **115**, 3164–3171.

35 R. Gupta and B. Rai, *Scientific Reports*, 2017, **7**, 1–13.

36 R. Gupta and B. Rai, *Journal of Physical Chemistry B*, 2016, **120**, 7133–7142.

37 D. Van Der Spoel, E. Lindahl, B. Hess, G. Groenhof, A. E. Mark and H. J. Berendsen, *Journal of Computational Chemistry*, 2005, **26**, 1701–1718.

38 C. Das, M. G. Noro and P. D. Olmsted, *Soft Matter*, 2014, **10**, 7346–7352.

39 A. Del Regno and R. Notman, *Physical Chemistry Chemical Physics*, 2018, **20**, 2162–2174.

40 L. Martinez, R. Andrade, E. G. Birgin and J. M. Martínez, *Journal of Computational Chemistry*, 2009, **30**, 2157–2164.

41 O. Berger, O. Edholm and F. Jähnig, *Biophysical Journal*, 1997, **72**, 2002–2013.

42 R. Notman, J. Anwar, W. J. Briels, M. G. Noro and W. K. den Otter, *Biophysical Journal*, 2008, **95**, 4763–71.

43 W. L. Jorgensen and J. Tirado-Rives, *Journal of the American Chemical Society*, 1988, **110**, 1657–1666.

44 F. W. van Gunsteren, S. R. Billeter, A. A. Eising, P. H. Hünenberger, P. Krüger, A. E. Mark, W. R. P. Scott and I. G. Tironi, *Biomolecular Simulation: The GROMOS96 Manual and User Guide*, 1996, pp. 1–1042.

45 J. P. Ryckaert and A. Bellemans, *Chemical Physics Letters*, 1975, **30**, 123–125.

46 D. Peter Tieleman, H. J. Berendsen and M. S. Sansom, *Biophysical Journal*, 1999, **76**, 1757–1769.

47 U. Essmann, L. Perera, M. L. Berkowitz, T. Darden, H. Lee and L. G. Pedersen, *The Journal of Chemical Physics*, 1995, **103**, 8577–8593.

48 B. Hess, H. Bekker, H. J. C. Berendsen and J. G. Fraaije, *J. Comput. Chem.*, 1997, **18**, 1463–1472.

49 G. Bussi, D. Donadio and M. Parrinello, *Journal of Chemical Physics*, 2007, **126**, 014101.

50 S. Jo, H. Rui, J. B. Lim, J. B. Klauda and W. Im, *Journal of Physical Chemistry B*, 2010, **114**, 13342–13348.

51 A. Bacle, R. Gautier, C. L. Jackson, P. F. Fuchs and S. Vanni, *Biophysical Journal*, 2017, **112**, 1417–1430.

52 A. Hall, J. Repakova and I. Vattulainen, *Journal of Physical Chemistry B*, 2008, **112**, 13772–13782.